



ELSEVIER

Computer Physics Communications 144 (2002) 317–342

---

---

Computer Physics  
Communications

---

---

www.elsevier.com/locate/cpc

# Shock capturing by anisotropic diffusion oscillation reduction

G.W. Wei

*Department of Computational Science, National University of Singapore, Singapore 117543*

Received 16 October 2001; received in revised form 17 January 2002

---

## Abstract

This paper introduces an anisotropic diffusion oscillation reduction (ADOR) scheme for shock wave computations. The connection is made between digital image processing, in particular, image edge detection, and numerical shock capturing. Indeed, numerical shock capturing can be formulated on the lines of iterative digital edge detection. Various anisotropic diffusion and super diffusion operators originated from image edge detection are proposed for the treatment of hyperbolic conservation laws and near-hyperbolic hydrodynamic equations of change. The similarity between anisotropic diffusion and artificial viscosity is discussed. Physical origins and mathematical properties of the artificial viscosity are analyzed from the point of view of kinetic theory. A form of pressure tensor is derived from the first principles of the quantum mechanics. Quantum kinetic theory is utilized to arrive at macroscopic transport equations from the microscopic theory. Macroscopic symmetry is used to simplify pressure tensor expressions. The latter provides a basis for the design of artificial viscosity. The ADOR approach is validated by using (inviscid) Burgers' equation, the gas tube problems, the incompressible Navier–Stokes equation and the Euler equation. Both standard central difference schemes and a discrete singular convolution algorithm are utilized to illustrate the approach. Results are compared with those of third-order upwind scheme and essentially non-oscillatory (ENO) scheme. © 2002 Published by Elsevier Science B.V.

---

## 1. Introduction

Shock wave is a common phenomenon in nature, such as in aerodynamics and hydrodynamics. Mathematically, nonlinear hyperbolic conservation equations provide a good description to shock waves. The construction of numerical schemes that are capable of shock capturing for hyperbolic and inviscid hydrodynamic equations is a major objective of computational methodology. However, it is noted that the concept of discontinuity does not apply in digital computations. Therefore, a shock in computational sense may refer to systematic, rapid variation of function values over a few grid points. The difficulty is that hyperbolic equation may have weak solutions that are discontinuous at the so-called shock front. Such a discontinuity will cause Gibbs' oscillations in a high (spatial) order numerical scheme. The numerically induced oscillations are usually amplified in (time) iterations. A variety of numerical schemes have been proposed for shock capturing. As early as 50 years ago, a solution to this problem was constructed by von Neumann and Richtmyer [1]. The essence of their approach is to introduce small artificial viscosity so that a smooth solution can always be attained in a finite difference

---

*E-mail address:* cscweigw@nus.edu.sg (G.W. Wei).

0010-4655/02/\$ – see front matter © 2002 Published by Elsevier Science B.V.

PII: S0010-4655(02)00273-4

approximation. A variety of modifications to von Neumann and Richtmyer's method are made in the past 5 decades to address problems of possible failure in spatial scaling and errors due to additional momentum flux and production, as well as unbalanced heat flux and its over production in the simulation of hyperbolic conservation laws.

A different approach was proposed by Godunov [2] to construct a full solution by using low order piecewise discontinuous approximations. Such a piecewise solution is a good approximation at the smooth regions, and is capable of representing the shock front over a small region of grid. The knowledge of wave propagation and wave interaction is built in the numerical scheme in the form of a Riemann solver. Godunov's approach has been extended to higher-order schemes [3–5]. In doing so, a higher-order approximation is constructed in the smooth region, while near the shock the solution is still of first order accuracy. The Godunov method is very stable and thus, easy to design and use [6]. However the major disadvantage of this method is the complexity introduced into a numerical scheme through a Riemann solver. Such a drawback reduces its computational efficiency.

Another general approach is the hybrid scheme, which utilizes a high-order scheme for a smooth region while using a low-order scheme near a discontinuity. A linear combination of these two types of schemes is then used at each interface using weight factors which may be nonlinear functions of the local flow field. DeBar constructed a linear hybridization of first-order and second-order difference schemes as early as 1968 [7]. Harten and Zwas [8] devised another early linear hybridization scheme. Boris and Book reported a blending algorithm which yields sharp discontinuities without oscillations [9]. A total variation diminishing (TVD) scheme was proposed by Harten [10] to control the spurious oscillations in the numerical solution by using the total variation as a measure. The TVD scheme typically degenerates to first-order accuracy at locations with smooth extreme and was later generalized to an essentially non-oscillatory (ENO) scheme [11–13]. The major idea of the ENO scheme is to suppress spurious oscillations near the shock or discontinuities, while maintaining a higher-order accuracy at smooth regions. This line of thinking was further polished recently in a weighted essentially non-oscillatory (WENO) scheme [14]. The WENO approach takes a linear combination of a number of high-order schemes of both central difference and up-wind types. The central difference type schemes have a larger weight factor at the smooth region while the up-wind schemes play a major role at the shock or discontinuity. In general, these approaches might be expensive since checks are performed before making a decision at each grid point. In terms of accuracy, all existing methods are at best of first order near the shock or discontinuity.

Perhaps modified artificial viscosity methods are the most popular approaches in practical computations. Unfortunately, the artificial viscosity smears shocks over three or more grid zones, which can lead to serious errors in the physical interpretation of the numerical results. Special care is required to ensure that the smeared numerical shock is consistent with the true thickness of the shock in a practical problem under study. This difficulty has led to enormous and continuous effort at developing efficient and robust approaches. One approach is to locally refine the computational grid [15]. An alternative approach is the use of an adaptive mesh [16,17]. Both methods are aimed at matching between the physical shock and the numerically smoothed one with respect to the spatial extension. These methods might have a restriction for extremely small time step sizes as required by the Courant constraint. In many cases, they need to be formulated in an implicit scheme, which might impose an extra complexity in practical implementation and an extra requirement in computer memory. Another possible problem is the unbalanced momentum flux and production, and additional heat flux and heat production in hydrodynamic equations. However, it is possible to find a good balance between the quality of shock-capturing and local refinement.

The addition of a viscous term to the inviscid hydrodynamic equations or the hyperbolic equation has a physical justification, that the true physical flow has no discontinuities. Therefore, mathematical model can be modified so as to reflect the true physics. In their original work, von Neumann and Richtmyer [1] have introduced an artificial viscosity  $q_{NR}$  of the form

$$q_{NR} \sim (\nabla \cdot \mathbf{v})^2 \quad (1)$$

for the equation of motion. Their term is of second order in gradient of the velocity field  $\mathbf{v}$  (the velocity gradient is a second rank tensor and has the divergence of velocity as its component) and will not be very sensitive to small gradients. Landshoff [18] proposed an additional term that vanishes less rapidly for small gradients

$$q_L \sim \nabla \cdot \mathbf{v}. \quad (2)$$

A generic form that contains both  $q_{NR}$  and  $q_L$  (i.e.  $\alpha \nabla \cdot \mathbf{v} + \beta (\nabla \cdot \mathbf{v})^2$ ) has been carefully studied by many researchers [19–22]. In particular, Caramana et al. [22] discussed a number of intuitive criteria for this form and the parameterization of artificial viscosity. Special considerations are given to dissipativity, Galilean invariance, self-similar motion invariance, wave front invariance and viscous force continuity. This generic form, as it was proposed for hydrodynamic conservation laws, has its advantages over other approaches for certain fluid mechanical computations. However, it is very unstable for certain hyperbolic equations due to the Courant–Friedrich–Lewy (CFL) stability condition. For example, it does not work well in resolving a sharp shock front for inviscid Burgers' equation with a smooth initial condition. We believe that this failure is due to the high-order in the gradient of the Neumann and Richtmyer form, which is too sensitive to large gradients at a sharp shock front. Despite the fact that a number of functional forms of the artificial viscosity have been proposed, the procedure is still ad hoc. For a given form, parameter selection is quite tricky and often varies from problem to problem.

The existence of so many different approaches for shock capturing indicates both the importance and the difficulty of the problem. The objective of the present paper is to introduce an anisotropic diffusion oscillation reduction (ADOR) approach for shock wave computations. The method of anisotropic diffusion in association with a partial differential equation was proposed by Perona and Malik [23] for digital image processing in 1990. Since then, much research has been stimulated in image processing and applied mathematics communities [24–34]. The method uses the heat equation, which has a solution of the Gaussian type, as a low pass filter to eliminate noise in an image, while it detects and preserves the edges of the image. It has been shown that the Perona–Malik equation provides a computational approach to image segmentation, noise removal, edge detection, and image enhancement. In a recent work, a generalized Perona–Malik equation was proposed for image restoration and edge enhancement [35]. In fact, digital edge detection has much in common with numerical shock capturing. In this work, we introduce a set of generalized anisotropic diffusion operators and edge enhancing functionals for shock wave computations.

This paper is organized as follows: Section 2 is devoted to kinetic theory analysis of the equation of change and artificial viscosity. The physical origin and mathematical properties of artificial viscosity are discussed from the kinetic theory point of view. A set of hydrodynamic equations describing fluid flow consisting of microscopic particles is derived from the quantum Boltzmann equation, i.e. the Waldmann–Snider equation [36,37]. The latter can be regarded as a consequence of a reduction of the von Neumann equation, or the quantum Liouville equation to the level of a single particle density operator. The mathematical form of the pressure tensor is analyzed by using the group theory consideration. A set of generalized artificial viscosities, artificial heat and artificial viral correction are proposed as the results of the kinetic theory analysis. Generalized Perona–Malik equation is discussed in Section 3 for shock wave computations. This approach follows a very different line of thinking as it was originally proposed for image analysis and processing. An edge-controlled image enhancing functional is introduced for shock representation. Anisotropic diffusion and diffusion superoperators are introduced for fast and effective shock capturing. Numerical experiments are presented in Section 4. A few standard test problems, including Burgers' equation and inviscid Burgers' equation in one- and two-dimension, the gas tube problems, the incompressible Euler and Navier–Stokes equations are used for exploring usefulness, testing efficiency and illustrating the validity of the ADOR approach. The implementation of the proposed approach has been done with both a recently developed discrete singular convolution (DSC) algorithm [38–43] and standard central difference schemes. The DSC algorithm is a unified approach for numerical computations [41] and its results are compared with those obtained by using high-order finite difference schemes. This paper ends with a conclusion.

## 2. Kinetic theory analysis of artificial viscosity

Artificial viscosity was originally proposed for shock capturing in association with hydrodynamic equations in the fluid mechanics. The choice of its form and parameter should be consistent with and motivated by the physical origin of hydrodynamic equations. Since quantum theory is the foundation for the modern fluid mechanics, a microscopic analysis is presented for appropriate understanding from the kinetic theory. The latter, such as the Boltzmann equation, serves as a theoretical basis for hydrodynamic conservation laws.

### 2.1. Microscopic analysis

Consider the flow of a quantum gas system consisting of total  $N$  particles in a volume  $S$ . Its behavior is governed by the Schrödinger equation

$$i\hbar \frac{\partial \Psi}{\partial t} = H^{(N)} \Psi, \quad (3)$$

where  $H^{(N)}$  is the self-adjoint Hamiltonian of the system and  $\Psi$  is a vector in the Hilbert space associated with the system. For the description of physical observable, we adopt the density operator  $\rho^{(N)}$  whose time evolution is governed by the quantum Liouville equation

$$i \frac{\partial \rho^{(N)}}{\partial t} = \mathcal{L}^{(N)} \rho^{(N)} = \frac{1}{\hbar} [H^{(N)}, \rho^{(N)}]_- = \frac{1}{\hbar} (H^{(N)} \rho^{(N)} - \rho^{(N)} H^{(N)}). \quad (4)$$

A physical observable  $O^{(N)}$  is a Hermitian operator of the Hilbert space and has the expectation value given by

$$\langle O^{(N)} \rangle = \text{Tr}_{1,\dots,N} O^{(N)} \rho^{(N)}, \quad (5)$$

where  $\text{Tr}_{1,\dots,N}$  is the trace over all the states of the  $N$ -particle system and in particular,

$$\langle 1^{(N)} \rangle = \text{Tr}_{1,\dots,N} 1^{(N)} \rho^{(N)} = 1 \quad (6)$$

gives the normalization of the total probability for finding all of the  $N$  particles in the volume  $S$ . Here  $1^{(N)}$  is the identity operator of the system. A standard form for the Hamiltonian is given by

$$H^{(N)} = K^{(N)} + V^{(N)} = \sum_i K_i + \sum_{i < j} V_{ij}, \quad (7)$$

where  $K_i$  is the kinetic energy (including internal state energy) operator of particle  $i$  and  $V_{ij}$  is the potential operator of particles  $i$  and  $j$ . The physical behavior of the  $N$ -particle system is far too complicated to compute by any means as a macroscopic gas flow may consist of  $10^{23}$  particles or more. Fortunately, for ordinary gases, it is sufficient to consider the state of a typical particle, say particle 1

$$\rho_1^{(1)} = N \text{Tr}_{2,\dots,N} \rho^{(N)}. \quad (8)$$

In general, the state of  $n$  particles is defined

$$\rho_{1,\dots,n}^{(n)} = N(N-1) \cdots (N-n+1) \text{Tr}_{n+1,\dots,N} \rho^{(N)}. \quad (9)$$

The time evolution of particle 1 is governed by

$$i \frac{\partial \rho_1^{(1)}}{\partial t} = \mathcal{L}^{(1)} \rho_1^{(1)} + \text{Tr}_2 \mathcal{V}_{12}^{(2)} \rho_{12}^{(2)} = \frac{1}{\hbar} [H^{(1)}, \rho_1^{(1)}]_- + \frac{1}{\hbar} \text{Tr}_2 [V_{12}, \rho_{12}^{(2)}]_-, \quad (10)$$

where  $H^{(1)} = K_1$ . This is the first member of the BBGKY hierarchy [44,45] in the quantum form. The general form of the BBGKY hierarchy [44,45] is given by

$$i \frac{\partial \rho_{1,\dots,n}^{(n)}}{\partial t} = \mathcal{L}^{(n)} \rho_{1,\dots,n}^{(n)} + \text{Tr}_2 \mathcal{V}_{1,\dots,n+1}^{(n+1)} \rho_{1,\dots,n+1}^{(n+1)}, \quad (11)$$

where  $\mathcal{V}_{1,\dots,n+1}^{(n+1)}$  is the potential superoperator between particles  $1, \dots, n$  and particle  $n + 1$ . This set of equations is formal and exact, since no approximation has been made. However, to determine the time evolution of  $\rho_1^{(1)}$ , it is necessary to know the behavior of  $\rho_{12}^{(2)}$ , which is, in turn, determined by the second order BBGKY equation and the latter involves three-particle density operator  $\rho_{123}^{(3)}$ .

## 2.2. Mesoscopic analysis

Kinetic theory attempts to explain macroscopic properties in terms of microscopic properties of the atoms and/or molecules based on the classical or quantum mechanics. Typical macroscopic observations deal with  $N$  ( $\sim 10^{23}$ ) particles over a volume much larger than the size of the individual molecules, and over a time period much longer compared to the time scale of the individual molecular dynamics. An ab-initio description of the time dependence of such macroscopic observations from the quantum Liouville equation is practically impossible not only because of the conceptual difficulty with the meaning of measurement, but also due to the large number of degrees of freedom involved. The kinetic theory approach simplifies the  $N$ -particle problem dramatically by looking at the behavior of one typical particle under the influence of all other particles.

The most successful kinetic theory has been based on the Boltzmann equation [36,37,46,47]. Specifically this has been related to the hydrodynamic equations and has given rise to molecular expressions for the transport coefficients. Various attempts have been made to understand the Boltzmann equation from the  $N$ -body Liouville equation, or utilizing the BBGKY hierarchy described in the last subsection. A first principle “derivation” of the Boltzmann equation from the Liouville equation has been achieved by Bogoliubov [45], and independently by Green [48]. The Wang Chang–Uhlenbeck–de Boer equation [49] was the first attempt to generalize the quantum Boltzmann equation, and to account for the internal degrees of freedom of a polyatomic gas. It was not generally realized until 1957 that polyatomic gases can only be treated properly by a quantum mechanical method due to the fact that the internal energy levels of such molecules are, in general, degenerate. Waldmann [36] and, independently, Snider [37] introduced a quantum kinetic equation, the Waldmann–Snider equation,

$$i \frac{\partial \rho_1^{(1)}}{\partial t} = \mathcal{L}_1^{(1)} \rho_1^{(1)} + \text{Tr}_2 \mathcal{V}_{12}^{(2)} \Omega_{L12} \rho_1^{(1)} \rho_2^{(1)}, \quad (12)$$

where  $\Omega_{L12}$  is the Møller superoperator for quantum mechanical scattering

$$\Omega_{L12} = \lim_{t \rightarrow -\infty} e^{i\mathcal{L}_{12}^{(2)}t} e^{-i\mathcal{K}_{12}^{(2)}t}, \quad (13)$$

where  $\mathcal{L}_{12}^{(2)}$  and  $\mathcal{K}_{12}^{(2)}$  are two-particle space Liouville operators for full interaction and kinetic motion, respectively. The Waldmann–Snider equation is still the basis for the kinetic theory of quantum gas flow [50–53]. Note that a dramatically simplified version of the Boltzmann equation provides the (lattice) Boltzmann gas (LBG) approach for the computational fluid dynamics in recent years.

## 2.3. Macroscopic analysis

The most important properties of a fluid flow are physical observables, or physical measurements. For conservative observables, the equations of change of physical observables give rise to conservation laws. The equations of change are important not only because they govern the time dependencies of the macroscopic quantities but also because they are needed for solving kinetic equations using the Chapman–Enskog method [54]. The equations of change for physical observables are derived in this subsection.

A single-particle observable for particle 1 is denoted by  $\psi_1$ . The expectation value of the physical observable  $\psi_1$  is determined by the singlet density operator  $\rho_1^{(1)}$  according to

$$\langle \psi_1 \rangle = \text{Tr}_1 \psi_1 \rho_1^{(1)}. \quad (14)$$

The most important physical observables are the number density  $n_1$ , stream velocity  $\mathbf{v}_1$  and kinetic energy  $\varepsilon_1^K$ . Firstly, the physical observable for the number density  $n_1$  is the Dirac delta distribution  $\psi_1 = \delta_1 \equiv \delta(\mathbf{r} - \mathbf{r}_1)$  so that

$$n_1 = \langle \delta_1 \rangle. \quad (15)$$

Secondly, the stream velocity  $\mathbf{v}_1$  is given by

$$\mathbf{v}_1 \equiv \frac{1}{n_1} \text{Tr}_1 \frac{1}{2m_1} (\mathbf{p}_1 \delta_1 + \delta_1 \mathbf{p}_1) \rho_1, \quad (16)$$

where  $m_1$  is the mass of particle 1. Finally, the kinetic energy  $\varepsilon_1^K$  per particle is given by

$$\varepsilon_1^K \equiv \frac{1}{n_1} \text{Tr}_1 \left( \frac{1}{8m_1} (\mathbf{p}_1^2 \delta_1 + 2\mathbf{p}_1 \cdot \delta_1 \mathbf{p}_1 + \delta_1 \mathbf{p}_1^2) - \frac{1}{2} m_1 \mathbf{v}_1^2 \delta_1 \right) \rho_1. \quad (17)$$

These expressions are appropriately symmetrized to account for the fact that position and momentum do not commute, while a physical observable is a Hermitian operator. Although this operator approach is used here for the number density  $n_1$ , stream velocity  $\mathbf{v}_1$  and kinetic energy  $\varepsilon_1^K$ , phase space expressions can be easily obtained for these fluid dynamic quantities by using the standard Wigner representation. The equations of change are of course independent of the detailed method used for the expression of various quantities. Equations of change for a particle observable is obtained from the quantum Boltzmann equation (12) according to

$$\frac{\partial \langle \psi_1 \rangle_1}{\partial t} - \left\langle \frac{\partial \psi_1}{\partial t} \right\rangle_1 = \frac{1}{i\hbar} \langle [\psi_1, H^{(1)}]_- \rangle_1 + \frac{1}{i} \text{Tr}_{1,2} \mathcal{V}_{12}^{(2)} \Omega_{L_{12}} \rho_1^{(1)} \rho_2^{(1)}. \quad (18)$$

In case that a physical observable  $\psi_1$  is time independent, the second term on the left-hand side of Eq. (18) vanishes. Conservation laws are the equation of continuity

$$\frac{\partial n_1}{\partial t} = -\nabla \cdot (n_1 \mathbf{v}_1), \quad (19)$$

the equation of motion

$$n_1 m_1 \frac{\partial \mathbf{v}_1}{\partial t} + n_1 m_1 \mathbf{v}_1 \cdot \nabla \mathbf{v}_1 = -\nabla \cdot \mathbf{P}_1, \quad (20)$$

and the kinetic energy equation

$$\frac{\partial n_1 \varepsilon_1^K}{\partial t} = -\nabla \cdot (n_1 \mathbf{v}_1 \varepsilon_1^K + \mathbf{q}_1^K + \mathbf{q}_{\text{coll}}) - \mathbf{P}_1^t : \nabla \mathbf{v}_1 + \sigma^K, \quad (21)$$

where the superscript  $t$  denotes the transpose and the kinetic heat flux is

$$\mathbf{q}_1^K = \text{Tr}_1 \left\{ \left( \frac{\mathbf{p}_1}{m_1} - \mathbf{v}_1 \right) \frac{(\mathbf{p}_1 - m_1 \mathbf{v}_1)^2}{2m_1} \delta_1 \right\}_s \rho_1, \quad (22)$$

where  $\{ \}_s$  designates appropriately operator-symmetrized quantities. Here the collisional heat flux is

$$\mathbf{q}_{\text{coll}} \equiv -\frac{1}{8m_1} \text{Tr}_{12} \int_{-1}^1 dv \left\{ \delta \left[ \mathbf{r} - \frac{\mathbf{r}_1 + \mathbf{r}_2}{2} - \frac{v}{2} (\mathbf{r}_1 - \mathbf{r}_2) \right] (\mathbf{p}_1 + \mathbf{p}_2 - 2m_1 \mathbf{v}_1) \cdot \frac{\partial V_{12}}{\partial \mathbf{r}_1} \right\}_s \Omega_{L_{12}} \rho_1^{(1)} \rho_2^{(1)} \quad (23)$$

and the kinetic energy production results from the collisional transfer of energy

$$\sigma^K = -\frac{1}{8m_1} \text{Tr}_{12} \left\{ (\delta_1 + \delta_2) \left[ (\mathbf{p}_1 - \mathbf{p}_2) \cdot \frac{\partial V_{12}}{\partial \mathbf{r}_1} + \frac{\partial V_{12}}{\partial \mathbf{r}_1} \cdot (\mathbf{p}_1 - \mathbf{p}_2) \right] \right\}_s \Omega_{L_{12}} \rho_1^{(1)} \rho_2^{(1)}. \quad (24)$$

The pressure tensor  $\mathbf{P}_1$  has kinetic and collisional contributions

$$\mathbf{P}_1 = \mathbf{P}_1^K + \mathbf{P}_1^{\text{coll}}, \quad (25)$$

where the kinetic pressure tensor is

$$\mathbf{P}_1^K \equiv \frac{1}{4m_1} \langle \delta_1 \mathbf{p}_1 \mathbf{p}_1 + \mathbf{p}_1 \delta_1 \mathbf{p}_1 + (\mathbf{p}_1 \delta_1 \mathbf{p}_1)^t + \mathbf{p}_1 \mathbf{p}_1 \delta_1 \rangle_1 - n_1 m_1 \mathbf{v}_1 \mathbf{v}_1 \quad (26)$$

and the collisional pressure tensor is given by

$$\mathbf{P}_1^{\text{coll}} = -\frac{1}{4} \text{Tr}_{12}(\mathbf{r}_1 - \mathbf{r}_2) \nabla_1 V_{12} \int_{-1}^1 \delta \left( \frac{\mathbf{r}_1 + \mathbf{r}_2}{2} + \frac{\nu}{2} (\mathbf{r}_1 - \mathbf{r}_2) - \mathbf{r} \right) dv \Omega_{L_{12}} \rho_1^{(1)} \rho_2^{(1)}. \quad (27)$$

The transpose  $\mathbf{P}_1^t$  of the pressure tensor  $\mathbf{P}_1$  enters to couple the convective energy to the internal kinetic energy per particle  $\varepsilon_1^K$ , heat flux contributions arise from kinetic  $\mathbf{q}_1^K$  and collisional  $\mathbf{q}_{\text{coll}}$  motion and finally there is a production term  $\sigma^K$  which involves the transfer between kinetic and potential energies. Although the equations of continuity and motion are consistent with the conservation of the number of particles and total momentum in the absence of bound pairs, the presence of the production term in the kinetic energy implies that the total kinetic energy is not conserved because of the possible conversion to potential energy due to the non-locality of the collisions (in the macroscopic sense). Thus it is necessary to look at the equation of change for the potential energy per particle  $\varepsilon_1^V$

$$n_1 \varepsilon_1^V = \frac{1}{4} \text{Tr}_{12}(\delta_1 + \delta_2) V_{12} \rho_{12}^{(2)}. \quad (28)$$

This is obtained in a manner consistent with pair particle interactions and shown to be of the form

$$\frac{\partial n_1 \varepsilon_1^V}{\partial t} = -\nabla \cdot (n_1 \mathbf{v}_1 \varepsilon_1^V + \mathbf{q}_1^V) - \sigma^K, \quad (29)$$

where

$$\mathbf{q}_1^V = \frac{1}{4m_1} \text{Tr}_{12}[(\mathbf{p}_1 - m_1 \mathbf{v}_1) \delta_1 + \delta_1 (\mathbf{p}_1 - m_1 \mathbf{v}_1)] V_{12} \Omega_{L_{12}} \rho_1^{(1)} \rho_2^{(1)}. \quad (30)$$

The production of potential and kinetic energy exactly cancels and there is an added heat flux contribution  $\mathbf{q}_1^V$  associated with the conductive potential energy flow.

In the next subsection, we show that an appropriate treatment of the pressure tensor leads to a method for shock capturing.

#### 2.4. Pressure tensor and artificial viscosity

The estimation of transport coefficients from the Boltzmann equation is quite complicated and involves many aspects. The most important transport quantities for physical and engineering applications are the mass, momentum and energy. Sometimes angular momentum transport may also be important for certain physical phenomena and thus an equation of change for angular momentum may be required. However, angular momentum conservation is rarely discussed in the context of hydrodynamic conservation laws. This is because the angular momentum is not measured like other physical observables in experiments. It is noted that all hydrodynamic conservation laws have the structure of convection, conduction and production. The equation of momentum conservation leads to shock wave as the divergence of the pressure tensor vanishes. The existence of shock wave devastates the numerical simulation as noted by von Neumann and Richtmyer [1]. They introduced artificial viscosity of the form of  $(\nabla \cdot \mathbf{v})^2$  to overcome the numerical difficulty. In fact, a much better choice can be selected by analyzing the form of the pressure tensor.

The pressure tensor is a tensor of second rank and has two indices. It has contributions from the kinetic transport  $\mathbf{P}^K$  and collision transport  $\mathbf{P}^{\text{coll}}$  (here, the subscript 1 is omitted for convenience). For example, the kinetic transport

$\mathbf{P}_{xy}^K$  is the rate of transport (kg m/s)/(m<sup>2</sup>s) in the  $x$ -direction, of the momentum with respect to the  $y$ -direction. The hydrodynamic pressure

$$\mathbf{P}_{\text{eq}} = nk_{\text{B}}T\mathbf{U}, \quad (31)$$

given by the equation of state, is the local equilibrium contribution to the pressure tensor. Here,  $\mathbf{U}$  is the identity tensor of second rank and  $k_{\text{B}}$  is the Boltzmann constant. In general, the gas is not at local equilibrium and the structure of the nonequilibrium part of the pressure tensor,

$$\mathbf{\Pi} = \mathbf{P} - \mathbf{P}_{\text{eq}} \quad (32)$$

can be analyzed according to the irreducible representation of the improper three-dimensional rotational group  $O(3)$ . As such,  $\mathbf{\Pi}$  can be expressed as a linear combination the irreducible representations

$$\mathbf{\Pi} = \Pi\mathbf{U} + \varepsilon \cdot \mathbf{P}^a + \mathbf{\Pi}^{(2)}, \quad (33)$$

where scalar, antisymmetric and symmetric traceless parts of the second rank tensor are given by

$$\begin{aligned} \Pi &= \frac{1}{3}\mathbf{U} : \mathbf{\Pi}, \\ \mathbf{P}^a &= -\frac{1}{2}\varepsilon \cdot \mathbf{\Pi}, \\ \mathbf{\Pi}^{(2)} &= \frac{1}{2}[\mathbf{\Pi} + \mathbf{\Pi}^t] - \frac{1}{3}\mathbf{U}[\mathbf{U} : \mathbf{\Pi}]. \end{aligned} \quad (34)$$

Here  $\varepsilon$  is the Levi–Civita tensor,  $\Pi$  is a scalar (one dimension),  $\mathbf{P}^a$  is a vector (three dimensions) and  $\mathbf{\Pi}^{(2)}$  is a tensor (five dimensions). In the theory of the Boltzmann equation and irreversible thermodynamics, the pressure tensor is treated as proportional to velocity gradient as in the case of a classical Newtonian flow. The velocity gradient,  $\nabla\mathbf{v}$ , is also a second rank tensor and can also be decomposed into three different components of order zero, one and two, similar to Eq. (34),

$$\begin{aligned} \nabla \cdot \mathbf{v} &= \frac{1}{3}\mathbf{U} : \nabla\mathbf{v}, \\ \nabla \times \mathbf{v} &= -\frac{1}{2}\varepsilon \cdot \nabla\mathbf{v}, \\ [\nabla\mathbf{v}]^{(2)} &= \frac{1}{2}[\nabla\mathbf{v} + (\nabla\mathbf{v})^t] - \frac{1}{3}\mathbf{U}\nabla \cdot \mathbf{v}. \end{aligned} \quad (35)$$

Here,  $\nabla\mathbf{v}$  is also a nine-dimensional quantity. In principle, there are 81 possible coefficients connecting the pressure tensor and the velocity gradient. Symmetry analysis indicates that there are three phenomenological equations relating the corresponding components of  $\mathbf{\Pi}$  and  $\nabla\mathbf{v}$

$$\begin{aligned} \Pi &= -\eta_V^0 \nabla \cdot \mathbf{v}, \\ \mathbf{P}^a &= -\eta_r^0 \nabla \times \mathbf{v}, \\ \mathbf{\Pi}^{(2)} &= -2\eta^0 [\nabla\mathbf{v}]^{(2)}, \end{aligned} \quad (36)$$

where  $\eta_V^0$ ,  $\eta_r^0$  and  $\eta^0$  are the viscosities of bulk, rotation and shear, respectively.

The pressure tensor given by Eq. (36) provides an excellent approximation for a gas system near the local equilibrium, i.e. the Boltzmann distribution

$$\rho_1^{(1)} = \frac{1}{\text{Tr}_1 e^{-K_1/k_{\text{B}}T}} e^{-K_1/k_{\text{B}}T}. \quad (37)$$

For the purpose of numerical stability and shock wave simulation, we can impose artificial pressure tensor as

$$\begin{aligned} \Pi_{\text{art}} &= -\zeta_V^0 \nabla \cdot \mathbf{v}, \\ \mathbf{P}_{\text{art}}^a &= -\zeta_r^0 \nabla \times \mathbf{v}, \\ \mathbf{\Pi}_{\text{art}}^{(2)} &= -2\zeta^0 [\nabla\mathbf{v}]^{(2)}, \end{aligned} \quad (38)$$

where  $\zeta_V^0$ ,  $\zeta_r^0$  and  $\zeta^0$  are artificial bulk viscosity, artificial rotational viscosity and artificial shear viscosity, respectively. These artificial viscosities only modify the non equilibrium part of the pressure tensor. In fact, from the point of view of computations, the equilibrium part of the pressure tensor can also be modified, i.e. a term which is proportional to  $nk_B T$

$$\mathbf{P}_{nT} = \epsilon nk_B T \mathbf{U}. \tag{39}$$

$\mathbf{P}_{nT}$  can be interpreted either as artificial heat or artificial viral correction. However, it should be noted that there is an advantage in keeping only the part of the artificial pressure tensor that corresponds to the non-equilibrium pressure tensor. The latter makes no additional contribution to conservative quantities, such as, number density, momentum and energy, as required by the Fredholm alternative for the existence of a solution for the kinetic equation in the Chapman–Enskog method [54]. Hence, we have the artificial pressure tensor of the form

$$\mathbf{P}_{art} = \Pi_{art} \mathbf{U} + \varepsilon \cdot \mathbf{P}_{art}^a + \mathbf{\Pi}_{art}^{(2)} \tag{40}$$

$$= -\zeta_V^0 \nabla \cdot \mathbf{v} \mathbf{U} - \zeta_r^0 \varepsilon \cdot \nabla \times \mathbf{v} - 2\zeta^0 [\nabla \mathbf{v}]^{(2)}. \tag{41}$$

Moreover, for a gaseous system far from the local equilibrium, higher-order terms in the velocity gradient become important. Large velocity gradient can build up from special boundary condition, such as the boundary layer phenomena, or from the lack of relaxation in a very dilute gas flow. Therefore artificial viscosities and artificial heat of Eqs. (38) can be modified to include higher-order velocity gradient contributions. Recognizing that the pressure tensor is a second rank tensor, thus all velocity gradients contribute in one of the forms of  $\Pi$ ,  $\mathbf{P}^a$  and  $\mathbf{\Pi}^{(2)}$ . In this regard, the artificial viscosity form proposed by von Neumann and Richtmyer [1],  $(\nabla \cdot \mathbf{v})^2$ , contributes to  $\Pi$ . Certainly, artificial viscosities of the forms of  $\nabla \cdot \mathbf{v}$ ,  $\nabla \times \mathbf{v}$  and  $[\nabla \mathbf{v}]^{(2)}$  can be used for numerical computations. All of the aforementioned forms are at least of first order in gradient, which may lead to a strong smearing at the edge of a shock front and thus lead to large errors in numerical applications. Furthermore, these forms can result in instability when the shock front is very sharp, such as in inviscid Burgers’ equation. For these reasons, it is appropriate to propose a general expression for the artificial viscosity and artificial heat so as to allow all coefficients to be functions of  $\nabla \cdot \mathbf{v}$ ,  $\nabla \times \mathbf{v}$  and  $[\nabla \mathbf{v}]^{(2)}$

$$\zeta_V^0 = \zeta_V^0(\nabla \cdot \mathbf{v}, \|\nabla \times \mathbf{v}\|, \|[\nabla \mathbf{v}]^{(2)}\|), \tag{42}$$

$$\zeta_r^0 = \zeta_r^0(\nabla \cdot \mathbf{v}, \|\nabla \times \mathbf{v}\|, \|[\nabla \mathbf{v}]^{(2)}\|), \tag{43}$$

$$\zeta^0 = \zeta^0(\nabla \cdot \mathbf{v}, \|\nabla \times \mathbf{v}\|, \|[\nabla \mathbf{v}]^{(2)}\|), \tag{44}$$

where  $\|\cdot\|$  denotes the magnitude and is computed as

$$\|\mathbf{A}\| = \sqrt{\frac{1}{N_A} \sum_i A_i^2} \tag{45}$$

for a vector  $\mathbf{A}$ , and

$$\|\mathbf{B}\| = \sqrt{\frac{1}{N_B} \sum_{ij} B_{ij}^2} \tag{46}$$

for a tensor  $\mathbf{B}$ . Here  $N_A$  and  $N_B$  are the dimensions of the vector  $\mathbf{A}$  and tensor  $\mathbf{B}$ , respectively. Obviously, artificial viscosity of von Neumann and Richtmyer [1],  $(\nabla \cdot \mathbf{v})^2$ , becomes a special case of the present treatment. The von Neumann and Richtmyer form can be classified as an artificial bulk viscosity term,  $\Pi_{art} \mathbf{U}$ .

The inclusion of an artificial rotational viscosity can be an efficient way for the treatment of fast rotational flow. It is noted that the rotational viscosity is in the original Navier–Stokes equation derived from the kinetic theory. However, for flows with natural boundary conditions, the angular momentum is also conserved and it does not couple the linear momentum except through internal spinor relaxations. However, this is no longer the

case in a flow with an irregular geometry. For such a case, the internal conversion between angular momentum and linear momentum is substantial and therefore the rotational viscosity,  $\eta_r^0$ , should be retained in both theoretical modeling and numerical simulation. A detailed discussion and numerical simulation of this aspect will be accounted elsewhere.

With this theoretical analysis of the pressure tensor, the equation of motion, i.e. Eq. (20), can be simplified as

$$\frac{\partial \mathbf{v}}{\partial t} + \mathbf{v} \cdot \nabla \mathbf{v} = -\nabla p + \frac{\eta^0}{nm} \nabla^2 \mathbf{v} + \frac{\eta_V^0 + \frac{1}{3}\eta^0}{nm} \nabla \nabla \cdot \mathbf{v} + \frac{\zeta^0}{nm} \nabla^2 \mathbf{v} + \frac{\zeta_V^0 + \frac{1}{3}\zeta^0}{nm} \nabla \nabla \cdot \mathbf{v}, \quad (47)$$

where  $p = \frac{1}{m} k_B T$  is the kinematic pressure. The molecular subscript in Eq. (20) has been omitted. Obviously, the conventional Navier–Stokes equation used for engineering computations consists of the first four terms of Eq. (47) with  $nm/\eta^0 = \text{Re}$ , the Reynolds number. The present kinetic theory leads to additional relaxation of the stream velocity from the bulk and shear viscosities. In an Euler (inviscid) flow ( $\eta^0 = \eta_V^0 = 0$ ), the artificial pressure tensor introduced in the present work can be utilized to stabilize the computation.

A lengthy but very similar discussion leads to a simplification to Eqs. (21) and (29), and the resulting equation for the temperature  $T$  is given by

$$\frac{\partial T}{\partial t} = -\mathbf{v} \cdot \nabla T - \frac{k_B T}{C_v} \nabla \cdot \mathbf{v} + \frac{\lambda^0}{nC_v} \nabla^2 T + \frac{\Lambda^0}{nC_v} \nabla^2 T, \quad (48)$$

where  $C_v = \frac{3}{2}k_B + C_{\text{int}}$  is the heat capacity,  $C_{\text{int}}$  is the internal heat capacity,  $\lambda^0$  is the thermal conductivity and  $\Lambda^0$  is the artificial thermal conductivity, which can be a nonlinear function of  $\nabla T$  in general. This set of equations can be used as a starting point for the numerical computations of shock waves. In the next section, we analyze the shock capturing algorithm further from the point of view of image processing, particularly, image edge detection.

### 3. Oscillation reduction by anisotropic diffusion

Although anisotropic diffusion was originally proposed for image processing, there is much in common between digital image processing and computational fluid dynamics. An image function  $I(\mathbf{r})$  is a two-dimensional projection of certain physical quantities, such as matter, velocity, energy, electromagnetic field, etc., under appropriate illumination conditions. The edges in an image usually refer to rapid changes in some physical properties, such as geometry, illumination, and reflectance. Mathematically, a discontinuity may be involved in the function representing such physical properties. Therefore image edges are very similar to shocks in fluid dynamics. Numerical shock capturing can be formulated on the lines of iterative digital edge detection. Edge detection is a key issue in image processing, computer vision, and pattern recognition. A variety of algorithms, such as the Sobel operator, the Prewitt operator, the Canny operator [55] and the DSC algorithm [56] are proposed for image edge detection and representation. Anisotropic diffusion is a promising new mathematical algorithm for image edge detection and image processing. This basic idea can be adopted and modified for numerical shock capturing in association with the hyperbolic conservation laws. The Perona–Malik algorithm [23] is reviewed before the method of anisotropic diffusion oscillation reduction (ADOR) is discussed.

#### 3.1. The Perona–Malik equation

The basic idea behind the Perona–Malik algorithm is to evolve an original image,  $I(\mathbf{r})$ , under an edge-controlled diffusion operator [23]

$$\frac{\partial u(\mathbf{r}, t)}{\partial t} = \nabla \cdot [d(\|\nabla u(\mathbf{r}, t)\|) \nabla u(\mathbf{r}, t)], \quad (49)$$

$$u(\mathbf{r}, 0) = I(\mathbf{r}).$$

Here,  $d(\|\nabla u\|)$  is a generalized diffusion coefficient which is so designed that its values are very small at the edges of an image. Many edge stopping functions  $d(|\nabla u|)$  are appropriate for anisotropic diffusion. For example, the Gaussian

$$d(\|\nabla u\|) = e^{-|\nabla u|^2/2\sigma^2} \quad (50)$$

and the Lorentz

$$d(\|\nabla u\|) = \frac{1}{1 + |\nabla u|^2/\sigma^2} \quad (51)$$

are both suitable for edge representation. They provide perceptually similar results in practical applications. Numerically, the diffusion coefficient becomes very small near an image edge due to the effect of edge stopping functions  $d(\|\nabla u\|)$ . As a result, the image edge is preserved in the diffusion process. The pixel values at a non-edge part will be smoothed and reduced due to the substantial diffusion coefficient prescribed by  $d(\|\nabla u\|)$ . Perona and Malik argued that the solution of their anisotropic diffusion equation has no additional maxima (minima) which does not belong to the initial image data. However, this point has been challenged recently [24,32]. It is well known that this anisotropic diffusion algorithm may break down when the gradient generated by noise is comparable to image edges and features. Numerically, this can be alleviated by using a regularization procedure.

### 3.2. Shock capturing by anisotropic diffusion

Hyperbolic conservation laws of the type

$$\frac{\partial u(\mathbf{r}, t)}{\partial t} + \nabla \cdot \mathbf{F}(u) = 0 \quad (52)$$

describe the rate of change of a physical quantity  $u$  given by the generalized convection  $\nabla \cdot \mathbf{F}(u)$ . Without the balance of conduction and/or production, Eq. (52) may have a discontinuous solution. The task is to construct a stable computational scheme which is capable of resolving the “shock”. We first note that computationally, if a shock is defined as a discontinuity, there is no shock to capture. This is because, the original notion of discontinuity is undefined on a discrete mesh. Therefore, a numerical shock is characterized by rapid variation of function values over a small grid zone. Numerical shock capturing, at best, is globally a first order approximation scheme for resolving the large gradient feature of the true solution. However, locally, it is preferred to compute the solution as accurate as possible, except at the discontinuity of the true solution. To this end, we introduce an anisotropic diffusion term to Eq. (52)

$$\frac{\partial u(\mathbf{r}, t)}{\partial t} + \nabla \cdot \mathbf{F}(u) = \nabla \cdot [d_1(\|\nabla u(\mathbf{r}, t)\|)\nabla u(\mathbf{r}, t)], \quad (53)$$

where the diffusivity,  $d_1(\|\nabla u(\mathbf{r}, t)\|)$ , is chosen such that it is essentially zero except at a numerical shock position. Obviously,  $\|\nabla u(\mathbf{r}, t)\|$  is important for shock detection. Apparently, Eq. (53) reduces to the Perona–Malik equation (49) without the convection term. However, the selections of the anisotropic diffusivity in these two equations are entirely different and serve opposite purposes. For example, one may choose  $d_1(\|\nabla u(\mathbf{r}, t)\|)$  as

$$d_1 = d_1^1 \ln[(\nabla u)^2 + 1], \quad (54)$$

where  $d_1^1$  is a constant. Eq. (54) differs much from the Gaussian and the Lorentz.

The derivation of Eq. (53) has its roots in the conservation of a physical quantity involving a phenomenological flux and its divergence. However, as a computational algorithm, an anisotropic diffusion of the form

$$\frac{\partial u(\mathbf{r}, t)}{\partial t} + \nabla \cdot \mathbf{F}(u) = \Gamma_1(\|\nabla u(\mathbf{r}, t)\|)\nabla^2 u(\mathbf{r}, t) \quad (55)$$

can be used. In fact, expressions in both Eqs. (53) and (55) are efficient for numerical shock capturing. Here,  $\Gamma_1$  is chosen to smooth the oscillations near a shock and is essentially zero in other regions.

### 3.3. Edge enhancing functional and super diffusion

From the hydrodynamic point of view, the governing equation of a conservative quantity has a general structure, i.e. the rate of change is balanced by convection, conduction and production. Therefore, the nonlinear advective motion can be counterbalanced by an appropriate production. Therefore, we propose a real-valued, bounded shock (edge) enhancing functional

$$e(\|\nabla u(\mathbf{r}, t)\|). \quad (56)$$

Here  $e(\|\nabla u(\mathbf{r}, t)\|)$  is appropriately chosen so that it is edge sensitive and is essentially zero away from a numerical shock or “discontinuity”. This leads to another shock capturing equation

$$\frac{\partial u(\mathbf{r}, t)}{\partial t} + \nabla \cdot \mathbf{F}(u) = \nabla \cdot [d_1(\|\nabla u(\mathbf{r}, t)\|)\nabla u(\mathbf{r}, t)] + e(\|\nabla u(\mathbf{r}, t)\|). \quad (57)$$

Appropriate choice of the shock enhancing functional will result in a stable numerical algorithm. Obviously, the von Neumann and Richtmyer [1] artificial viscosity term, Eq. (1), is a special case of the present formulation.

The diffusion equation can be derived from Fick’s law for mass flux,

$$\mathbf{j}_1(\mathbf{r}, t) = -D_1 \nabla u(\mathbf{r}, t) \quad (58)$$

with  $D_1$  being a constant. From the point of view of kinetic theory, this is an approximation to a quasi homogeneous system which is near equilibrium. A better approximation can be expressed as a super flux

$$\mathbf{j}_q(\mathbf{r}, t) = -\sum_q D_q \nabla \nabla^{2q} u(\mathbf{r}, t) \quad (q = 1, 2, \dots), \quad (59)$$

where  $D_q$  are constants and higher order terms ( $q > 1$ ) describe corrections to mass flux by the influence of inhomogeneity in density distribution and of flux–flux correlations. The mass conservation leads to

$$\begin{aligned} \frac{\partial u(\mathbf{r}, t)}{\partial t} &= -\nabla \cdot \mathbf{j}_q(\mathbf{r}, t) + s(\mathbf{r}, t) \\ &= \sum_q \nabla \cdot [D_q \nabla \nabla^{2q} u(\mathbf{r}, t)] + s(\mathbf{r}, t) \quad (q = 1, 2, \dots), \end{aligned} \quad (60)$$

where  $s$  is a source term which can be a nonlinear function describing chemical reactions. Eq. (60) is a generalized reaction-diffusion equation which includes not only the usual diffusion and production terms, but also super diffusion terms. A truncation at the second order super flux,  $\mathbf{j}_2(\mathbf{r}, t) = -D_1 \nabla u(\mathbf{r}, t) - D_2 \nabla \nabla^2 u(\mathbf{r}, t)$ , leads to the expression that is important in many phenomenological theories, such as the Cahn–Hilliard equation and the Kuramoto–Sivashinsky equation. The latter have been used for the description of a number of physical phenomena, such as the Taylor–Couette flow, parametric waves and pattern formation in alloys, glasses, polymers, combustion and biological systems [57].

In a shock wave simulation process, the distribution of the physical quantity under study can be highly inhomogeneous and/or oscillatory. Hence, the present shock capturing algorithm can be made more efficient by incorporating a shock (edge) sensitive super diffusion operator

$$\begin{aligned} \frac{\partial u(\mathbf{r}, t)}{\partial t} + \nabla \cdot \mathbf{F}(u) &= \sum_q \nabla \cdot [d_q(\|\nabla u(\mathbf{r}, t)\|)\nabla \nabla^{2q} u(\mathbf{r}, t)] \\ &+ e(\|\nabla u(\mathbf{r}, t)\|) \quad (q = 1, 2, \dots). \end{aligned} \quad (61)$$

Here  $d_q(u, |\nabla u|)$  are shock (edge) sensitive diffusion functions. In most applications, a truncation at  $q = 2$  is sufficient

$$\begin{aligned} \frac{\partial u(\mathbf{r}, t)}{\partial t} + \nabla \cdot \mathbf{F}(u) &= \nabla \cdot [d_1(\|\nabla u(\mathbf{r}, t)\|)\nabla u(\mathbf{r}, t)] \\ &+ \nabla \cdot [d_2(\|\nabla u(\mathbf{r}, t)\|)\nabla \nabla^2 u(\mathbf{r}, t)] \\ &+ e(\|\nabla u(\mathbf{r}, t)\|). \end{aligned} \quad (62)$$

This equation can be simplified further for practical implementation

$$\begin{aligned} \frac{\partial u(\mathbf{r}, t)}{\partial t} + \nabla \cdot \mathbf{F}(u) &= \Gamma_1(\|\nabla u(\mathbf{r}, t)\|)\nabla^2 u(\mathbf{r}, t) \\ &+ \Gamma_2(\|\nabla u(\mathbf{r}, t)\|)\nabla^4 u(\mathbf{r}, t) \\ &+ e(\|\nabla u(\mathbf{r}, t)\|), \end{aligned} \quad (63)$$

where  $\Gamma_1$  and  $\Gamma_2$  are to be appropriately chosen to capture the shock. Usually,  $\Gamma_1$  is a positive function, while  $\Gamma_2$  is negative.

From the point view of image processing, both operators  $\nabla^2$  and  $\nabla^4$  are high pass filters. In the Fourier representation, operators  $\nabla^2$  and  $\nabla^4$  are proportional to  $\omega^2$  and  $\omega^4$  of the frequency  $\omega$ . Hence,  $\nabla^2$  is more sensitive to low frequency oscillations while  $\nabla^4$  has a large filter response for high frequency oscillations. Although both  $\nabla^2$  and  $\nabla^4$  become band pass filters on a discrete grid, their filter responses have similar properties as in their abstract operator forms.

Note that many of these anisotropic terms presented in this section resemble those expressions derived in the last section for the artificial pressure tensor,  $\mathbf{P}_{\text{art}}$ . Obviously, for the Navier–Stokes equation,  $\Gamma_1$  of Eq. (63) is the same as  $\zeta^0/nm$  in Eq. (47). Although the starting points for these two approaches are entirely different, the results are obviously connected. Therefore, notations are to be simplified and possible confusions are to be avoided. For these reasons, we use the acronym ADOR for both approaches.

#### 4. Numerical experiments

In this section, the numerical schemes developed from the analysis of kinetic theory and image processing analysis are utilized for numerical computations involving shock waves. Parameter selections for the ADOR method are specified. Obviously, there are infinitely many ways to construct anisotropic diffusion functionals. For simplicity, we test the following choices of the ADOR coefficients:

$$d_1 = d_1^1 \ln[(\nabla u)^2 + 1], \quad d_2 = d_2^1 \ln[(\nabla u)^2 + 1], \quad e = e^1 (\nabla \cdot u)^2, \quad (64)$$

for Eq. (62),

$$\Gamma_1 = \gamma_1^1 (|u_x|)^{1/4}, \quad \Gamma_2 = \gamma_2^1 (|u_x|)^{1/4}, \quad e = 0, \quad (65)$$

for Eq. (63),

$$\Gamma_1 = \gamma_1^2 \ln[|u_x| + 1], \quad \Gamma_2 = \gamma_2^2 \ln[|u_x| + 1], \quad e = 0, \quad (66)$$

for Eq. (63),

$$\Gamma_1 = \gamma_1^3 \ln[u_x^2 + 1], \quad \Gamma_2 = \gamma_2^3 \ln[u_x^2 + 1], \quad e = 0, \quad (67)$$

for Eq. (63), and

$$\Gamma_1 = \gamma_1^4 \ln[\|\nabla u\| + 1], \quad \Gamma_2 = \gamma_2^4 \ln[\|\nabla u\| + 1], \quad e = 0, \quad (68)$$

for Eq. (63). In fact, coefficients in  $x$ - and  $y$ -direction can be chosen separately

$$\Gamma_1 = \gamma_1^5 \begin{cases} \ln[|u_x| + 1] & \text{for } u_{xx} \\ \ln[|u_y| + 1] & \text{for } u_{yy} \end{cases}, \quad \gamma_2^5 = 0, \quad e = 0. \quad (69)$$

Note that these expressions have one feature in common, i.e. they are all of low order in the gradient of  $u$ . This feature allows a sharp change in the solution to be handled by a coarse grid. Otherwise, if there are higher-order gradient terms, such as the von Neumann and Richtmyer form [1], the computational grid near the shock front has to be refined to reduce the flux amplitude. A finer grid, in turn, leads to another stability problem as dictated by the CFL condition.

In the rest of this section, the performance of the abovementioned prescriptions is examined for a detailed choice of ADOR parameters  $d_1^1, d_2^1, e^1$  and  $\gamma_j^i$  ( $i = 1, 2, 3; j = 1, 2$ ). A few standard problems are employed to test the validity, and to demonstrate the robustness of the present approach. These problems include Burgers' equation in one and two space dimensions, the gas tube problems, the incompressible Navier–Stokes equation and Euler equation with periodic boundary conditions.

The spatial discretization of the ADOR method is implemented with standard finite difference schemes [58] of order four (ADOR-FD4) and six (ADOR-FD6), and the discrete singular convolution (ADOR-DSC). The DSC algorithm was proposed as a potential approach for computer realization of singular convolutions [38–41]. Mathematical foundation of the algorithm is the theory of distributions [59]. Sequence of approximations to the singular kernels of Hilbert type, Abel type and delta type were constructed. Numerical solutions to differential equations are formulated via singular kernels of delta type. By appropriately choosing the DSC kernels, the DSC approach exhibits global methods' accuracy for integration and local methods' flexibility for handling complex geometries and boundary conditions. In particular, we demonstrated [41] that different implementations of the DSC algorithm, such as global, local, Galerkin, collocation, and finite difference, can be deduced from a single starting point. The DSC algorithm is validated for the numerical solution of the Fokker–Planck equation [38], the Schrödinger equation [40] and the Navier–Stokes equation [60,61]. It was also utilized to integrate the (nonlinear) sine-Gordon equation with the initial values close to a homoclinic orbit singularity [39], for which conventional local methods encounter great difficulties and numerically induced chaos was reported for such an integration [62]. The reader is referred to [38] for a detailed discussion of the method. The DSC parameters used in the present work are  $\sigma/\Delta = 3.2$  and  $M = 31$  for the DSC kernel of regularized Shannon [38]. For time discretization, the explicit 4th-order Runge–Kutta scheme is used for Burgers' equation and for the gas tube problems. The incompressible Navier–Stokes equation is integrated by using the implicit Euler scheme in association with a discrete singular convolution-alternating direction implicit (DSC-ADI) algorithm [63]. Further information is given in subsections below.

#### 4.1. Burgers' equation in one dimension

Burgers' equation [64] is an important model for the understanding of physical flows. It appears customary to test new schemes in computational fluid dynamics by applying them to Burgers' equation. Despite much of the effort, numerical solution of Burgers' equation is still not a trivial task, particularly at very high Reynolds numbers where the nonlinear advection leads to shock waves. In fact, many standard computational algorithms fail to predict Burgers' inviscid shocks.

Burgers' equation is given by

$$\frac{\partial u}{\partial t} + u \frac{\partial u}{\partial x} = \frac{1}{\text{Re}} \frac{\partial^2 u}{\partial x^2}, \quad (70)$$

where  $u(x, t)$  is the dependent variable resembling the flow velocity and Re is the Reynolds number characterizing the size of the viscosity. The competition between the nonlinear advection and the viscous diffusion is controlled by the value of Re in Burgers' equation, and thus determines the behavior of the solution.

4.1.1. Smooth initial values

We consider Burgers’ equation (70) with the following initial and boundary conditions

$$\begin{aligned}
 u(x, 0) &= \sin(\pi x), \\
 u(0, t) &= u(1, t) = 0.
 \end{aligned}
 \tag{71}$$

Cole has provided an exact solution [65] for this problem in terms of a series expansion which is readily computable roughly for the parameter  $Re \leq 100$ . For the parameter  $Re = 100$ , the present calculations use two sets of grid points ( $N = 51$  and  $101$ ) in the interval  $[0, 1]$  with a time increment of  $0.002$ . For a comparison, a third-order upwind scheme for convection, in association with a fourth-order central difference scheme for diffusion, is also utilized to solve this problem under the same discretization conditions. Both  $L_1$  and  $L_\infty$  errors of the DSC, FD4, FD6 and the upwind scheme are listed in Table 1. Obviously, the DSC is much more accurate than other schemes.

We next consider inviscid Burgers’ equation ( $Re = \infty$ ) with the same initial and boundary conditions as given in Eq. (71). In this case, the system does not admit analytical solution and the numerical solution quickly develops into a sharp shock front at  $x = 1$ . The DSC algorithm does not work along because severe oscillations eventually turn into an uncontrolled error growth. This problem is treated by using the anisotropic diffusion approach discussed in the previous sections. The performance of four different prescriptions given in Eqs. (64)–(67) is examined in association with the DSC algorithm. ADOR parameter selections are compared in Fig. 1 at 4 different times ( $t = 0.3, 0.5, 0.8, 2.0$ ). These results are all obtained by using 101 grid points with a time increment of  $0.002$ .

In Figs. 1(a)–1(d), there is essentially no difference among four different forms of anisotropic coefficients for the region away from the shock front. At the shock front  $x = 1$ , results computed from different forms are slightly different. Except for Fig. 1(b), there is a visible overshoot near the shock front at  $t = 2.0$  for all other forms of

Table 1  
A comparison of errors for solving Burgers’ equation

N	Time	DSC		FD4		FD6		Upwind	
		$L_1$	$L_\infty$	$L_1$	$L_\infty$	$L_1$	$L_\infty$	$L_1$	$L_\infty$
51	0.2	6.3(−05)	6.4(−04)	6.3(−05)	6.5(−04)	6.3(−05)	6.4(−04)	6.1(−05)	5.4(−04)
	0.6	1.4(−04)	2.5(−03)	1.1(−03)	5.1(−02)	6.3(−04)	2.5(−02)	9.5(−04)	1.8(−02)
	1.0	1.9(−05)	3.7(−04)	4.9(−04)	1.8(−02)	1.8(−04)	7.6(−03)	5.3(−04)	8.8(−03)
	1.4	1.9(−06)	3.3(−05)	2.0(−04)	5.8(−03)	5.5(−05)	2.0(−03)	2.8(−04)	3.6(−03)
	1.8	2.4(−07)	2.9(−06)	9.4(−05)	2.1(−03)	1.9(−05)	5.9(−04)	1.6(−04)	1.8(−03)
	2.2	5.6(−08)	7.6(−07)	5.1(−05)	8.9(−04)	7.9(−06)	2.0(−04)	9.6(−05)	9.5(−04)
	2.6	1.5(−08)	1.9(−07)	3.0(−05)	4.8(−04)	3.6(−06)	7.7(−05)	6.4(−05)	5.5(−04)
	3.0	3.3(−09)	4.6(−08)	1.9(−05)	2.7(−04)	1.8(−06)	3.3(−05)	4.4(−05)	3.5(−04)
101	0.2	6.3(−05)	1.5(−03)	6.3(−05)	1.5(−03)	6.3(−05)	1.5(−03)	6.3(−05)	1.6(−03)
	0.6	4.5(−07)	1.4(−05)	8.8(−05)	3.9(−03)	1.8(−05)	1.1(−03)	1.3(−04)	3.1(−03)
	1.0	2.7(−08)	7.1(−07)	3.5(−05)	1.2(−03)	4.9(−06)	2.3(−04)	6.7(−05)	1.3(−03)
	1.4	1.8(−09)	4.8(−08)	1.4(−05)	4.0(−04)	1.3(−06)	4.5(−05)	3.2(−05)	5.1(−04)
	1.8	9.8(−11)	3.1(−09)	6.5(−06)	1.4(−04)	4.1(−07)	1.3(−05)	1.8(−05)	2.4(−04)
	2.2	6.0(−12)	1.9(−10)	3.4(−06)	6.6(−05)	1.6(−07)	4.2(−06)	1.1(−05)	1.3(−04)
	2.6	6.7(−13)	1.3(−11)	2.0(−06)	3.2(−05)	6.8(−08)	1.5(−06)	7.4(−06)	7.2(−05)
	3.0	2.2(−13)	1.4(−12)	1.2(−06)	1.8(−05)	3.3(−08)	6.8(−07)	5.2(−06)	4.4(−05)

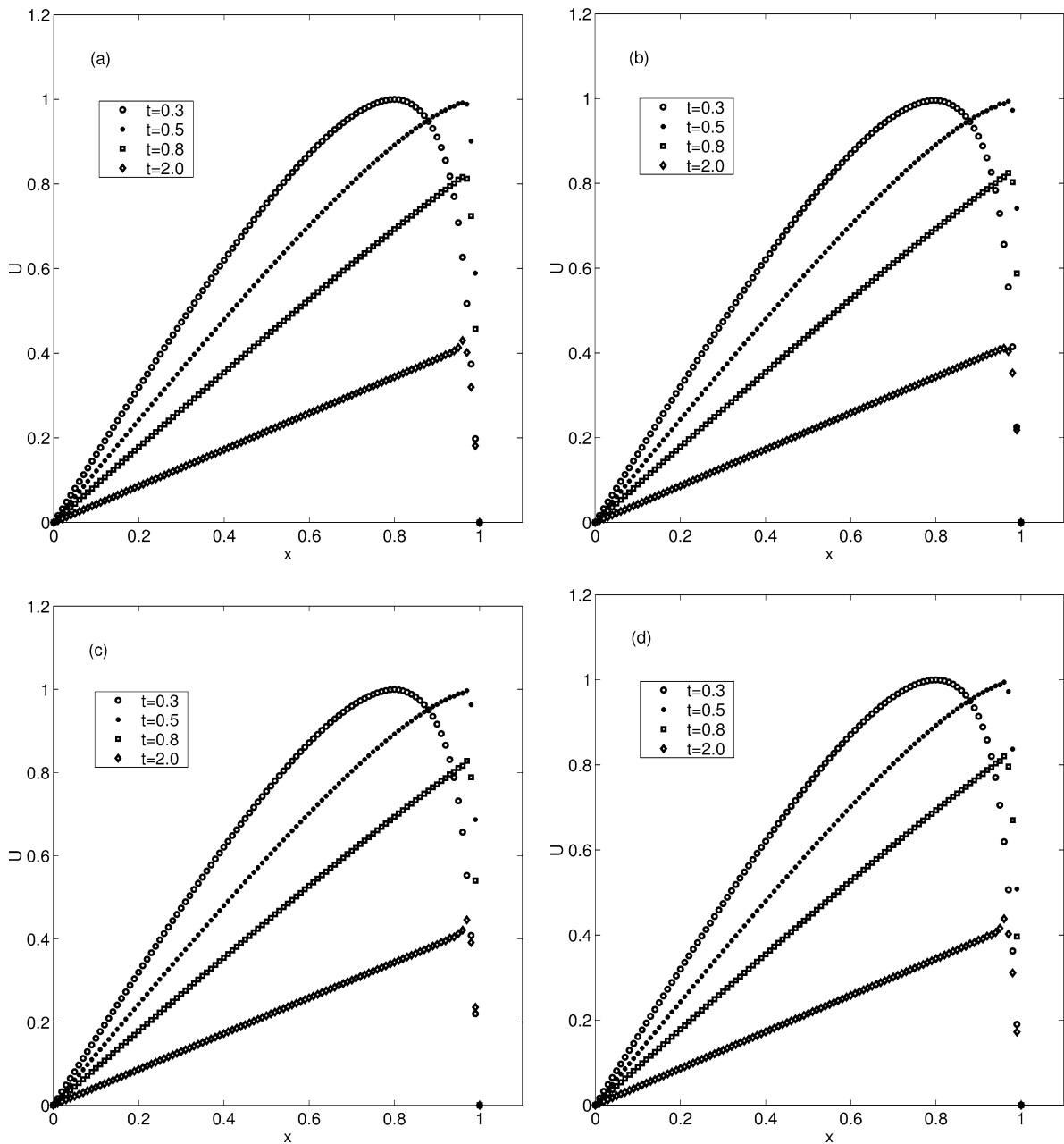


Fig. 1. A comparison of various ADOR coefficients for the numerical solution of inviscid Burgers' equation. (a)  $a_1^1 = 0.0009$ ,  $a_2^1 = 0$ ,  $e^1 = 0$ ; (b)  $\gamma_1^1 = 0.0022$ ,  $\gamma_2^1 = 0$ ; (c)  $\gamma_1^2 = 0.0018$ ,  $\gamma_2^2 = 0$ ; (d)  $\gamma_1^3 = 0.0015$ ,  $\gamma_2^3 = 0$ ; (e)  $\gamma_1^3 = 0$ ,  $\gamma_2^3 = -3 \times 10^{-8}$ .

anisotropic coefficients. Therefore, the scheme in Eq. (64) gives a better result. By refining the mesh, we have confirmed that all results are essentially correct and contain very little over-smearing. It is seen that all the four different choices of the diffusion coefficients have similar behavior and are all capable of correctly simulating Burgers' shock.

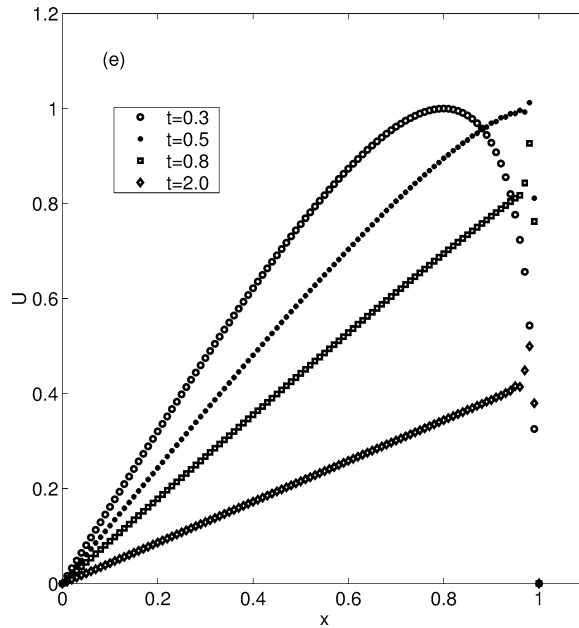


Fig. 1. (Continued.)

Fig. 1(e) depicts the results obtained by using the super diffusion coefficient as shown in Eq. (67). Obviously, it does not work very well since the shock front ( $x = 1$ ) is distorted and there are overshoots at  $t = 0.5, 0.8$  and  $2.0$ . In fact, we find that a combination of anisotropic diffusion and super diffusion does work better than the choice of a single term (results not shown). Similar results were also obtained by using 50 grid points. It is mentioned that the tests on the use of the edge enhancing functional does not result in a stable solution with the mesh system and time increment, chosen the present study.

#### 4.1.2. A Riemann type initial value

We further consider the inviscid ( $Re = \infty$ ) Burgers' equation (70) with a Riemann type initial value

$$u(x, 0) = \begin{cases} 1, & \text{if } 0 \leq x \leq 0.2, \\ 0, & \text{if } 0.2 < x \leq 1. \end{cases} \tag{72}$$

The exact solution is a shock front moving at a constant speed  $\frac{1}{2}$ . This discontinuous solution is a shock wave of compressive nature. This problem is chosen to compare the performance of the ADOR-DSC, ADOR-FD4, ADOR-FD6 and upwind. The spatial and temporal discretizations are the same as in the previous case (i.e. using 101 grid points in the interval of  $[0, 1]$  and a time increment of 0.002). The ADOR coefficients used are  $\gamma_1^1 = 0.001$  for ADOR-DSC,  $\gamma_1^1 = 0.002$  for ADOR-FD4 and ADOR-FD6. For a comparison, the third-order upwind scheme is utilized to solve this problem under the same discretization conditions. The results of the ADOR and upwind schemes are plotted in Fig. 2. The results of ADOR-FD4, ADOR-FD6 and ADOR-DSC are all very similar and they are very close to the exact solution. In particular, the result obtained by using the ADOR-DSC scheme has only two points located away from the exact solution. Such a result is as good as that obtained by using the state of the art schemes discussed in the introduction. Obviously, the third-order upwind scheme is not as effective as the ADOR approach for oscillation suppression. Since the ADOR scheme is not sensitive to different implementations, we focus on the ADOR-DSC in the rest of the paper.

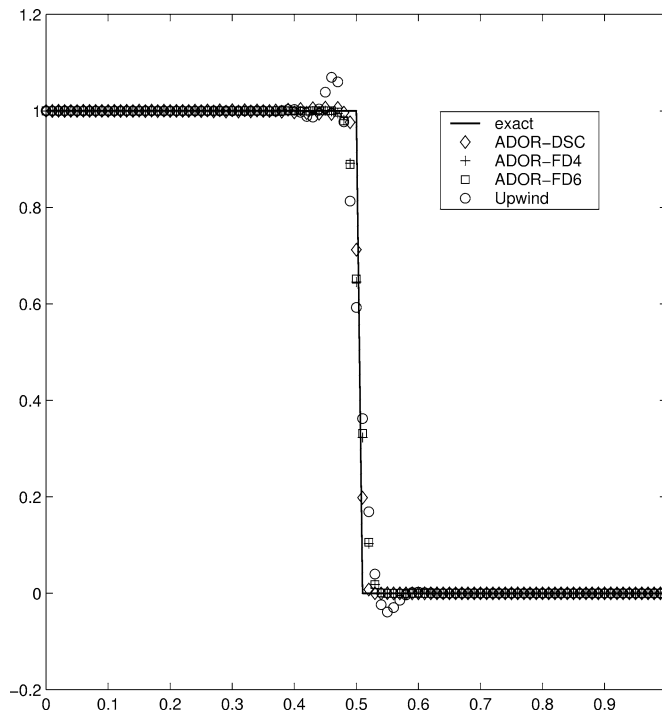


Fig. 2. The ADOR and upwind solutions for the inviscid Burgers' equation with a Riemann type initial value ( $t = 0.6$ ).

#### 4.2. Burgers' equation in two dimensions

Let us consider Burgers' equation of the form

$$u_t + uu_x + vv_y = \frac{1}{\text{Re}}(u_{xx} + u_{yy}), \quad (73)$$

$$v_t + uv_x + vv_y = \frac{1}{\text{Re}}(v_{xx} + v_{yy}) \quad (74)$$

in a square  $[0, 1] \times [0, 1]$  with the initial values

$$u(x, y, 0) = \sin(\pi x) \sin(\pi y), \quad (75)$$

$$v(x, y, 0) = [\sin(\pi x) + \sin(2\pi x)] + [\sin(\pi y) + \sin(2\pi y)] \quad (76)$$

and boundary conditions

$$u(0, y, t) = u(1, y, t) = u(x, 0, t) = u(x, 1, t) = 0, \quad (77)$$

$$v(0, y, t) = v(1, y, t) = v(x, 0, t) = v(x, 1, t) = 0. \quad (78)$$

This problem admits no analytical solution and is chosen to demonstrate that the present algorithm can be effective, even with a very coarse mesh. This case is computed by using an ADOR-DSC parameter of  $\gamma_1^4 = 0.02$ ,  $\gamma_2^4 = 0$  with  $41^2$  points. Since there is no exact solution for this problem, the convergence of the present solution is confirmed by systematically refining the mesh. The contours of velocity field components at  $t = 1$  are plotted in Fig. 3. Obviously, there is a shock at the up-right corner in both the  $u$  and  $v$  velocity fields.

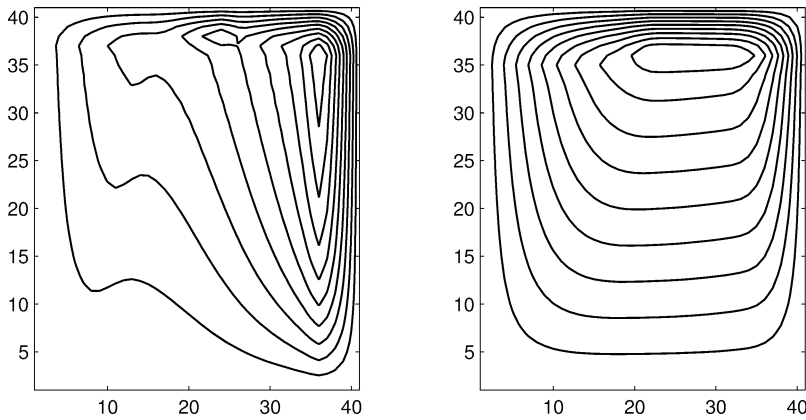


Fig. 3. The ADOR solution for the 2D inviscid Burgers' equation with  $41^2$  points,  $\gamma_1^4 = 0.02$ ,  $\gamma_2^4 = 0$ . Left: the  $u$  field; right: the  $v$  field.

### 4.3. The compressible Navier–Stokes equations

To further test the proposed scheme, we consider the compressible Navier–Stokes equations, which are special cases of the full Navier–Stokes equations, i.e. Eqs. (19), (47) and (48). The 1D Euler equations of gas dynamics take the form

$$\begin{bmatrix} \rho \\ \rho u \\ E \end{bmatrix}_t + \begin{bmatrix} \rho u \\ \rho u^2 + p \\ u(E + p) \end{bmatrix}_x = \mathbf{0}, \tag{79}$$

where  $\rho$  is the density,  $u$  the velocity,  $E$  the total energy,  $\gamma = 1.4$  a constant and  $p$  the pressure which is given by

$$p = (\gamma - 1)(E - \frac{1}{2}\rho u^2). \tag{80}$$

Two Riemann problems, the Sod problem and Lax problem [12], are employed to demonstrate the present ADOR approach. The initial data of Sod's problem are

$$\begin{aligned} \rho &= 1; & u &= 0; & p &= 1; & \text{when } x < 0, \\ \rho &= 0.125; & u &= 0; & p &= 0.1; & \text{when } x \geq 0. \end{aligned}$$

Similarly, the set of initial data for the Lax problem is given by

$$\begin{aligned} \rho &= 0.445; & u &= 0.698; & p &= 3.528; & \text{when } x < 0, \\ \rho &= 0.5; & u &= 0; & p &= 0.571; & \text{when } x \geq 0. \end{aligned}$$

These gas dynamic problems are non-trivial and are benchmark examples for testing new shock-capturing schemes. There is no exact solution in close-form for Riemann problems of the Euler equation. However, exact solutions are available for the present two problems via numerical iterations and are accurate to any desired practical degree. Hence, these problems are invaluable for assessing the performance of new shock-capturing methods [4,12]. The solution of both problems consists of a left rarefaction, a contact discontinuity and a right shock. The Sod problem is relatively easy to compute. However, the Lax problem is a very severe test. The ADOR scheme is applied to the density, velocity and kinetic energy, respectively. The prescription in Eq. (65) is used with the ADOR parameters of  $\gamma_2^1 = e = 0$  and  $\gamma_1^1 = 0.002, 0.005, 0.005$  for  $\rho, u$  and  $E$ , respectively in both problems. We note that slightly large anisotropic diffusion coefficients for the velocity and energy fields can result in a better effect for the contact discontinuity in the density profile. Numerical solutions at  $t = 2.0$  are shown in Fig. 4 for the Sod problem. A comparison of these solutions with the exact ones is also presented in the plot to evaluate the present ADOR

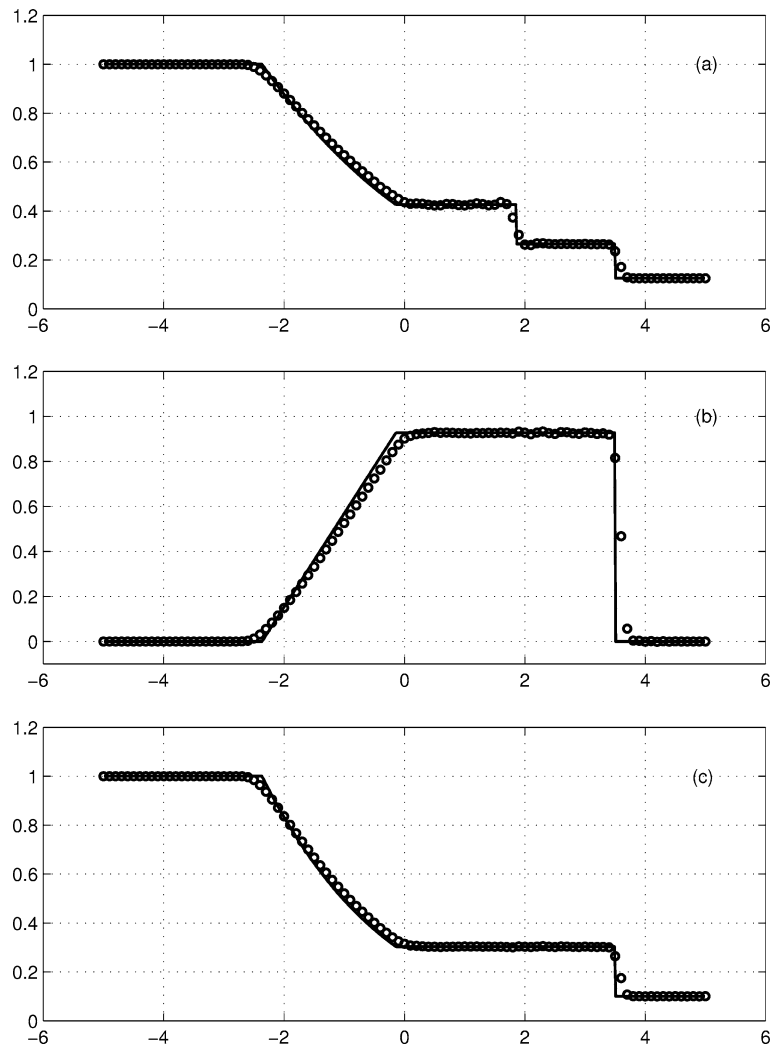


Fig. 4. Sod problem of the Euler system at  $t = 2.0$ ,  $\Delta x = 0.1$ ,  $\frac{\Delta t}{\Delta x} = 0.2$ . Solid lines: exact solution; circles: numerical results: (a) density; (b) velocity; (c) pressure.

scheme. It is seen that the proposed scheme work extremely well for the Sod problem. There are only two points of the numerical solution in midst of the contact or shock discontinuity. The ADOR results of density, velocity and pressure for the Lax problem are depicted in Fig. 5. The numerical solution of the density has only 4 points in the midst of contact discontinuity and 3 points in the midst of the right shock. These results are some of the best even obtained for this difficult gas tube problem.

#### 4.4. The incompressible Navier–Stokes equations

To test the present approach for shock capturing further for more complicated cases, we consider the velocity Navier–Stokes equation which is a simplified version of that discussed in Section 2

$$\frac{\partial \mathbf{v}}{\partial t} + \mathbf{v} \cdot \nabla \mathbf{v} = -\nabla p + \frac{1}{\text{Re}} \nabla^2 \mathbf{v}, \quad (81)$$

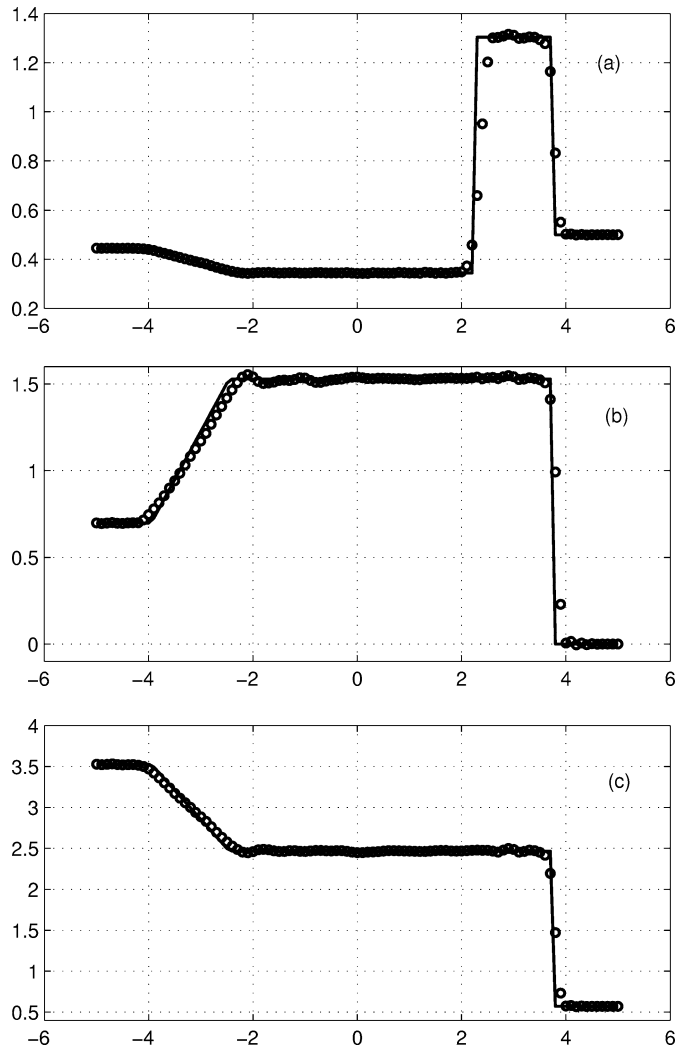


Fig. 5. Lax problem of the Euler system at  $t = 1.5$ ,  $\Delta x = 0.1$ ,  $\frac{\Delta t}{\Delta x} = 0.2$ . Solid lines: exact solution; circles: numerical results: (a) density; (b) velocity; (c) pressure.

where  $p$  is the pressure,  $\text{Re}$  ( $\text{Re} > 0$ ) is the Reynolds number and  $\text{Re} = \infty$  defines the Euler equation. For incompressible flow, the equation of continuity reduces to

$$\nabla \cdot \mathbf{v} = 0. \quad (82)$$

We solve these equations in two spatial dimensions, i.e.  $\mathbf{v} = (u, v)$ . The domain of problem is a square  $[0, 2\pi] \times [0, 2\pi]$  with periodic boundary conditions. With appropriate initial values, the Euler equation can be used to describe a flow field of vertically perturbed horizontal shear layers around a jet. Bell et al. [6] studied this case by a second order projection method. Recently E and Shu [13] have employed this example to demonstrate the success of their high order ENO scheme for resolving the fine vorticity structure of the double shear layers.

#### 4.4.1. Analytically solvable initial values

The Navier–Stokes equation is analytically solvable for appropriate initial values

$$\begin{aligned} u(x, y, 0) &= -\cos(x) \sin(y), \\ v(x, y, 0) &= \sin(x) \cos(y). \end{aligned} \quad (83)$$

The exact solution for this case is given by [13]

$$\begin{aligned} u(x, y, t) &= -\cos(x) \sin(y) e^{-2t/\text{Re}}, \\ v(x, y, t) &= \sin(x) \cos(y) e^{-2t/\text{Re}}, \\ p(x, y, t) &= -\frac{1}{4} [\cos(2x) + \cos(2y)] e^{-4t/\text{Re}}. \end{aligned} \quad (84)$$

This provides a benchmark test for potential numerical methods in fluid dynamics. The implicit Euler scheme is used for the time integration and the DSC algorithm is utilized for the spatial discretization. The accuracy and reliability of this combination was previously tested [60] for this problem using a standard LU decomposition algorithm for solving linear algebraic equations. Here, DSC-ADI algorithm [63] is used. We choose a grid of  $32^2$  for the present calculation with a time increment of 0.001. The DSC-ADI results are summarized in Table 2. Note that, for the inviscid case ( $\text{Re} = \infty$ ) the present result is accurate to the machine precision. It is evident that the accuracy of the DSC approach is extremely high, particularly when the Reynolds numbers are very large.

#### 4.4.2. The incompressible Euler equation

We now test the anisotropic diffusion approach for the incompressible Euler equation ( $\text{Re} = \infty$ ) with sharply varying initial values. This example is chosen to illustrate the ability of the present approach, for providing very fine resolution with a relatively coarse grid. The initial values are that of a jet in a doubly periodic geometry

$$\begin{aligned} u(x, y, 0) &= \begin{cases} \tanh\left(\frac{2y-\pi}{2\rho}\right), & \text{if } y \leq \pi, \\ \tanh\left(\frac{3\pi-2y}{2\rho}\right), & \text{if } y > \pi, \end{cases} \\ v(x, y, 0) &= \delta \sin(x), \end{aligned} \quad (85)$$

where  $\delta = 0.05$  is used for the convenience of comparison with the previous study [13]. This initial value describes the flow field consisting of horizontal shear layers of finite thickness, perturbed by a small amplitude vertical velocity, making up the boundaries of the jet. However, this problem is not analytically solvable. A pioneer work in this study was given by Bell et al. [6], in which they utilized a second-order Godunov scheme in association with a

Table 2

$L_2$  errors of the DSC-ADI solutions for the 2D Navier–Stokes equation computed with 32 grid point in each dimension

Re	$t = 1$		$t = 2$		$t = 3$		$t = 4$	
	$u$	$v$	$u$	$v$	$u$	$v$	$u$	$v$
20	6.1(-11)	6.1(-11)	1.1(-10) <sup>a</sup>	1.1(-10)	1.5(-10)	1.5(-10)	1.8(-10)	1.8(-10)
$10^2$	1.2(-12)	1.2(-12)	2.3(-12)	2.3(-12)	3.4(-12)	3.4(-12)	4.4(-12)	4.4(-12)
$10^3$	9.5(-13)	9.3(-13)	1.9(-12)	1.8(-12)	2.8(-12)	2.8(-12)	3.8(-12)	3.7(-12)
$10^4$	8.4(-13)	8.3(-13)	1.7(-12)	1.7(-12)	2.6(-12)	2.6(-12)	3.5(-12)	3.5(-12)
$10^5$	4.6(-13)	4.6(-13)	9.7(-13)	9.7(-13)	1.4(-12)	1.4(-12)	1.9(-12)	1.9(-12)
$10^6$	6.3(-13)	6.3(-13)	1.2(-12)	1.2(-12)	1.7(-12)	1.9(-12)	2.6(-12)	2.6(-12)
$\infty$	1.5(-15)	1.5(-15)	1.6(-15) <sup>b</sup>	1.6(-15)	1.6(-15)	1.6(-15)	1.7(-15)	1.7(-15)

<sup>a</sup>  $L_2 = 9.1(-04)$ ,

<sup>b</sup>  $L_2 = 4.9(-04)$  were reported in Ref. [13].

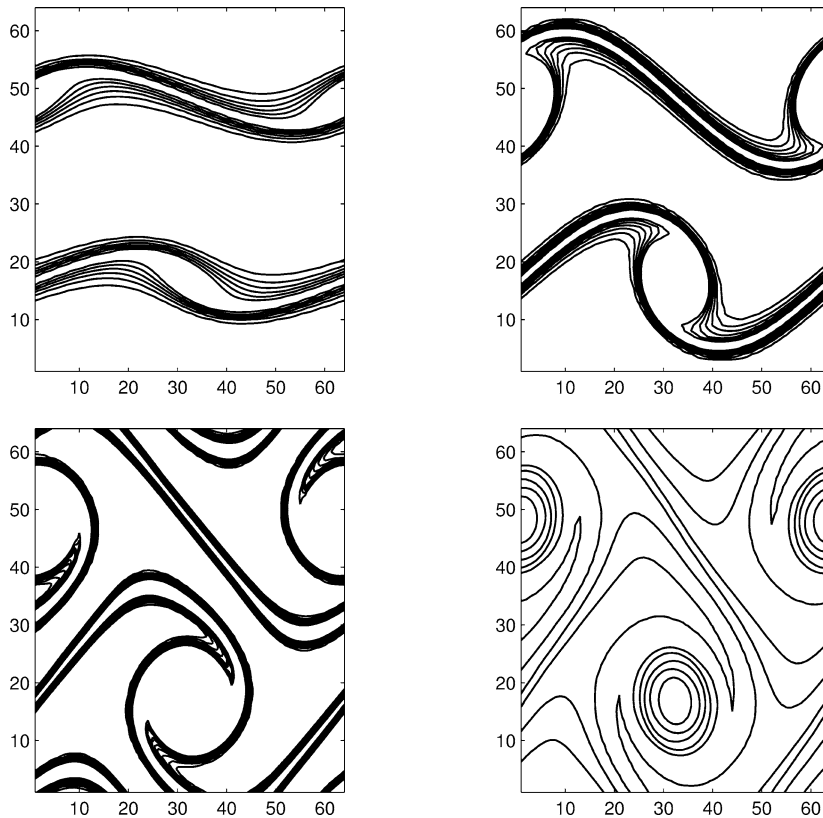


Fig. 6. The vorticity contours for the 2D Euler equation by the ADOR method with  $\gamma_1^3 = 0.0006$ . Up left:  $t = 4$ ; up right:  $t = 6$ ; low left:  $t = 8$ ; low right:  $t = 10$ .

projection approach for divergence-free velocity fields with general boundary condition. With a periodic boundary condition, E and Shu have shown that their high-order ENO scheme [13] performs well for this problem.

We consider the parameter  $\rho = \pi/15$ , a case studied by Bell et al. [6] using a projection method with three sets of grids ( $128^2$ ,  $256^2$  and  $512^2$ ). E and Shu [13] computed this case by using both spectral collocation code with  $512^2$  points and their high order ENO scheme with  $64^2$  and  $128^2$  points. The spectral collocation code produced an oscillatory solution at  $t = 10$  (see Fig. 1 of Ref. [13]), while the high order ENO scheme produced a defect at  $t = 6$  as the channels connecting the vorticity centers are slightly distorted (see Fig. 2 of Ref. [13]). In the present simulation, we choose a  $64^2$  grid for the computational domain with a time increment of 0.002. The prescription in Eq. (67) is used with the ADOR parameter of  $\gamma_1^3 = 0.0006$ . The results at different times ( $t = 4, 6, 8, 10$ ) are plotted in Fig. 6. It is seen that the present solutions are smooth (some non-smooth features in the contour plot is due to the fact that the grid is very coarse) and stable for this case. In particular, no distortion is found in vorticity contours at  $t = 6$ . For early times, present results compare extremely well with those of the spectral collocation code computed with  $512^2$  points. There are no spurious numerical oscillations during the entire process.

## 5. Conclusions

Connection is made between digital image processing and computational fluid dynamics. The evolution of an image surface under a partial differential operator can be viewed as a form of image processing. Computationally,

numerical shock capturing can be formulated on the lines of iterative edge-detection. Hence, techniques developed in the computational fluid dynamics can be used for image processing and vice-versa. This paper introduces the method of anisotropic diffusion oscillation reduction (ADOR), an approach which has its roots in image processing, for shock wave computations.

In fact, the ADOR method is much similar to the artificial viscosity algorithm. Physical origins and mathematical properties of the artificial viscosity are discussed from the point of view of kinetic theory. The form of pressure tensor is derived from the first principles of quantum mechanics. Quantum kinetic theory is utilized to arrive at macroscopic transport equations from the microscopic quantum theory. Macroscopic symmetry is used to simplify the phenomenological pressure tensor expressions. The latter provides the basis for the design of artificial viscosity. The original von Neumann–Richtmyer form of artificial viscosity fits into a special case of the present generalizations.

The anisotropic diffusion, which is essentially an image processing technique, is modified for shock capturing. The technique preserves image edges by introducing little diffusion, where the image gradient is large, while it provides a substantial diffusion coefficient at smooth parts of the image. In the present shock capturing algorithm, the edge-sensitive diffusion is introduced at a shock front so that large oscillations can be efficiently eliminated. An edge enhancing functional and edge-detected super diffusion operators are proposed for shock capturing. These terms are introduced from the general structure of conservation laws. In fact, kinetic theory analysis and anisotropic diffusion argument lead to a number of similar expressions for shock wave treatments. Hence, the acronym ADOR is referred for both approaches.

The reliability and robustness of the ADOR scheme is explored in association with the standard central difference schemes and the discrete singular convolution (DSC) algorithm [38–41]. It is found that the performance of the ADOR is not sensitive to different spatial discretizations. A few detailed prescriptions for the anisotropic diffusion functional are considered in this work. The coefficients in these prescriptions are chosen to be of lower order in gradient so that a coarse grid can be used. A number of standard test examples, including (inviscid) Burgers' equation in one and two spatial dimensions, the Sod problem, the Lax problem, the incompressible Navier–Stokes and the Euler equations, are employed for the present test computations. Our numerical results indicate that the proposed method works well for shock wave computations. The implementation of the present approach to more complex conservation law problems is under progress.

## Acknowledgement

This work was supported in part by the National University of Singapore. The author thanks Professor C.-W. Shu for useful discussions about the ENO and WENO schemes.

## References

- [1] J. von Neumann, R.D. Richtmyer, A method for the numerical calculation of hydrodynamic shocks, *J. Appl. Phys.* 21 (1950) 232.
- [2] S.K. Godunov, Finite difference method for numerical computation of discontinuous solutions to the equations of fluid dynamics, *Math. Sb.* 47 (1959) 271.
- [3] B. van Leer, Towards the ultimate conservative difference scheme. IV. A new approach to numerical convection, *J. Comput. Phys.* 23 (1977) 276.
- [4] P.R. Woodward, P. Collela, in: *Lecture Notes in Phys.*, Vol. 141, Springer-Verlag, New York, 1981, p. 434.
- [5] P.R. Woodward, P. Collela, The numerical simulation of two-dimensional fluid flow with strong shocks, *J. Comput. Phys.* 54 (1984) 115.
- [6] J.B. Bell, P. Cilella, H.M. Glaz, A second-order projection method for the incompressible Navier–Stokes equations, *J. Comput. Phys.* 85 (1989) 257.
- [7] R. DeBar, Fundamentals of the KRAKEN code, Lawrence Livermore National Laboratory Report UCIR-760, 1974.
- [8] A. Harten, G. Zwas, Self-adjusting hybrid schemes for shock computations, *J. Comput. Phys.* 6 (1972) 568.
- [9] J.P. Boris, D.L. Book, Flux-corrected transport. I. SHASTA, a fluid transport algorithm that works, *J. Comput. Phys.* 11 (1973) 38.

- [10] A. Harten, High resolution schemes for hyperbolic conservation law, *J. Comput. Phys.* 49 (1983) 357.
- [11] A. Harten, B. Engquist, S. Osher, S. Chakravarthy, Uniform high-order accurate essentially non-oscillatory schemes, III, *J. Comput. Phys.* 71 (1987) 231.
- [12] C.-W. Shu, S. Osher, Efficient implementation of nonoscillatory shock capturing schemes II, *J. Comput. Phys.* 83 (1989) 32.
- [13] W. E. C.-W. Shu, A numerical resolution study of high order essentially non-oscillatory schemes applied to incompressible flow, *J. Comput. Phys.* 110 (1994) 39.
- [14] X.-D. Liu, S. Osher, T. Chan, Weighted essentially non-oscillatory schemes, *J. Comput. Phys.* 115 (1994) 200.
- [15] W.D. Gropp, A test of moving mesh refinement for 2D scalar hyperbolic problems, *SIAM J. Sci. Statist. Comput.* 1 (1980) 191.
- [16] P. Eggleton, *Monthly Notices Roy. Astronom. Soc.* 151 (1971) 351.
- [17] R.J. Gelinias, S.K. Doss, K. Miller, *J. Comput. Phys.* 40 (1981) 202.
- [18] R. Landshoff, A numerical method for treating fluid flow in the presence of shocks, Los Alamos National Laboratory Report, LA-1930, 1955.
- [19] V.F. Kuropatenko, in: N.N. Janeko (Ed.), *Difference Methods for Solutions of Problems of Mathematical Physics*, Vol. 1, American Mathematical Society, Providence, 1967, p. 116.
- [20] M.L. Wilkins, Use of artificial viscosity in multidimensional shock wave problems, *J. Comput. Phys.* 36 (1980) 281.
- [21] W.D. Schulz, Two-dimensional Lagrangian hydrodynamic difference schemes, *Methods Comput. Phys.* 3 (1964) 1.
- [22] E.J. Caramana, M.J. Shashkov, P.P. Whalen, Formulations of artificial viscosity for multi-dimensional shock wave computations, *J. Comput. Phys.* 144 (1998) 70.
- [23] P. Perona, J. Malik, Scale-space and edge detection using anisotropic diffusion, *IEEE Trans. Pattern Anal. Machine Intell.* 12 (1990) 629.
- [24] F. Catte, P.-L. Lions, J.-M. Morel, T. Coll, Image selective smoothing and edge detection by nonlinear diffusion, *SIAM J. Numer. Anal.* 29 (1992) 182.
- [25] M. Nitzberg, T. Shiota, Nonlinear image filtering with edge and corner enhancement, *IEEE Trans. Pattern Anal. Machine Intell.* 14 (1992) 826.
- [26] L. Rudin, S. Osher, E. Fatemi, Nonlinear total variation base noise removal algorithm, *Physica D* 60 (1992) 259.
- [27] R.T. Whitaker, S.M. Pizer, A multi-scale approach to nonuniform diffusion, *CVGIP: Image Understanding* 57 (1993) 99.
- [28] Y.-L. You, W. Xu, A. Tannenbaum, M. Kaveh, Behavior analysis of anisotropic diffusion in image processing, *IEEE Trans. Image Process.* 5 (1996) 1539.
- [29] F. Torkamani-Azar, K.E. Tait, Image recovery using the anisotropic diffusion equation, *IEEE Trans. Image Process.* 5 (1996) 1573.
- [30] J. Shah, A common framework for curve evolution, segmentation and anisotropic diffusion, in: *IEEE Proc. Conf. Computer Vision and Pattern Recognition*, San Francisco, CA, June 1996, pp. 136–142.
- [31] S.T. Acton, Edge enhancement of infrared imagery by way of anisotropic diffusion pyramid, in: *IEEE Proc. 3rd Internat. Conf. Image Processing Lausanne*, Switzerland, Sept. 1996, pp. 865–868.
- [32] M. Kichenassamy, The Perona–Malik paradox, *SIAM J. Appl. Math.* 57 (1997) 1328.
- [33] S. Teboul, L. Blanc-Feraud, G. Aubert, M. Barlaud, Variational approach for edge-preserving regularization using coupled PDE's, *IEEE Trans. Image Process.* 7 (1998) 387.
- [34] M.J. Black, G. Sapiro, D.H. Marimont, D. Heeger, Robust anisotropic diffusion, *IEEE Trans. Image Process.* 7 (1998) 421.
- [35] G.W. Wei, Generalized Peron–Malik equation for image restoration, *IEEE Signal Proc. Lett.* 6 (1999) 165.
- [36] L. Waldmann, *Z. Naturforsch. A* 12 (1957) 660.
- [37] R.F. Snider, Quantum mechanical modified Boltzmann equation for degenerate internal states, *J. Chem. Phys.* 32 (1960) 1051.
- [38] G.W. Wei, Discrete singular convolution for the solution of the Fokker–Planck equations, *J. Chem. Phys.* 110 (1999) 8930.
- [39] G.W. Wei, Discrete singular convolution method for the sine-Gordon equation, *Physica D* 137 (2000) 247.
- [40] G.W. Wei, Solving quantum eigenvalue problems by discrete singular convolution, *J. Phys. B* 33 (2000) 343.
- [41] G.W. Wei, A unified approach for the solution of the Fokker–Planck equation, *J. Phys. A: Meth. Gen.* 33 (2000) 4935.
- [42] G.W. Wei, Vibration analysis by discrete singular convolution, *J. Sound Vibration* 244 (2001) 535.
- [43] G.W. Wei, Discrete singular convolution for beam analysis, *Engrg. Structures* 23 (2001) 1045.
- [44] M. Born, H.S. Green, *Proc. Roy. Soc. London A* 188 (1946) 10;  
J.G. Kirkwood, *J. Chem. Phys.* 14 (1946) 180;  
J. Yvon, *La Théorie Statistique des Fluides et l'Equation d'Etat*, Hermann, Paris, 1935.
- [45] N.N. Bogoliubov, *J. Phys. (USSR)* 10 (1946) 256.
- [46] L. Boltzmann, *Wein. Ber.* 66 (1872) 275 (Collected Works, Vol. 1, p. 315).
- [47] H. Grad, in: S. Flügge (Ed.), *Handbuch der Physik*, Springer Verlag, Berlin, 1958.
- [48] H.S. Green, *Molecular Theory of Fluids*, North-Holland, Amsterdam, 1952.
- [49] C.S. Wang Chang, G.E. Uhlenbeck, J. de Boer, in: J. de Boer, G.E. Uhlenbeck (Eds.), *Studies in Statistical Mechanics*, Vol. 2, North-Holland, Amsterdam, 1964.
- [50] F.R.W. McCourt, J.J.M. Beenakker, W.E. Köhler, I. Kuščer, *Nonequilibrium Phenomena in Polyatomic Gases*, Oxford Univ. Press, 1990.
- [51] R.F. Snider, A density corrected quantum Boltzmann equation, *J. Stat. Phys.* 61 (1990) 443.
- [52] R.F. Snider, G.W. Wei, J.G. Muga, Moderately dense gas quantum kinetic theory: Aspects of pair correlations, *J. Chem. Phys.* 105 (1996) 3057–3065.

- [53] R.F. Snider, G.W. Wei, J.G. Muga, Moderately dense gas quantum kinetic theory: Transport coefficient expressions, *J. Chem. Phys.* 105 (1996) 3066–3078.
- [54] S. Chapman, T.G. Cowling, *The Mathematical Theory of Non-Uniform Gases*, Cambridge Univ. Press, Cambridge, 1953.
- [55] Canny, A computational approach to edge detection, *IEEE Trans. Patt. Anal. Machine Intell.* PAMI-8 (1986) 679–698.
- [56] Z.J. Hou, G.W. Wei, A new approach to edge detection, *Pattern Recognition* 35 (7) (2002) 1559–1570.
- [57] M.C. Cross, P.C. Hohenberg, Pattern formation outside of equilibrium, *Rev. Modern Phys.* 65 (1993) 851.
- [58] B. Fornberg, *A Practical Guide to Pseudospectral Methods*, Cambridge University Press, 1966.
- [59] L. Schwartz, *Théorie des Distributions*, Hermann, Paris, 1951.
- [60] G.W. Wei, A new algorithm for solving some mechanical problems, *Comput. Methods Appl. Mech. Engrg.* 190 (2001) 343–352.
- [61] D.C. Wan, B.S.V. Patnaik, G.W. Wei, A new benchmark quality solution for the buoyancy driven cavity by discrete singular convolution, *Numer. Heat Transfer B: Fundamentals* 40 (2001) 199.
- [62] M.J. Ablowitz, B.M. Herbst, C. Schober, On numerical solution of the sine-Gordon equation, *J. Comput. Phys.* 126 (1996) 299.
- [63] Y.B. Zhao, G.W. Wei, Method of discrete singular convolution-alternating direction implicit, unpublished.
- [64] J. Burgers, A mathematical model illustrating the theory of turbulence, in: *Advances in Applied Mechanics*, Academic Press, 1948.
- [65] J.D. Cole, On a quasi-linear parabolic equation occurring in aerodynamics, *Quart. Appl. Math.* 9 (1951) 225.